Parametric Inversion Technique for Location of Cylindrical Structures by Cross-Hole Measurements

Kazunori Takahashi, *Student Member, IEEE*, and Motoyuki Sato, *Senior Member, IEEE*

Abstract—A new parametric inversion technique to locate cylindrical structures has been developed for borehole radar cross-hole measurements. The technique calculates prediction errors, focusing on curve shapes of first-arrival times, and explicitly uses known parameters on a target. Two schemes to compare the measured first-arrival time curves with the calculated ones are proposed. One is by taking the errors between curve gradients of measured and calculated first-arrival times, and the other is by taking the cross correlation between calculated first-arrival times and measured data. The schemes do not need to select the true first-arrival times, which makes this inversion technique robust and easy to use. This technique is validated with synthetic data sets modeling a metallic pipe in homogeneous and heterogeneous medium models. By both models, the inversion technique is able to retrieve the exact location of the pipe, though it employs a rather simple forward model, which can be solved by only geometrical calculations. The technique is applied to measured data sets, and it successfully estimates a pipe location in good agreement with known information. The inversion is also used for an air-filled subsurface cavity with a very simplified forward model, which considers only Snell's law at the cavity-subsurface media interface. It is also able to locate the cavity at a similar location estimated by other conventional techniques.

Index Terms—Borehole radar, cross-hole, ground-penetrating radar (GPR), inverse problem, pipe detection, tunnel detection.

I. INTRODUCTION

SURFACE ground-penetrating radar (GPR) has been broadly used in many applications in order to nondestructively investigate the subsurface, e.g., in geological and archeological surveys, for detecting buried objects and studying subsurface cavities, because of its easy usage, quick operation, and visualization capabilities. However, surface GPR cannot be used for deeper underground sensing due to the strong attenuation of electromagnetic waves in the subsurface medium. Borehole radar is generally used for such deep underground surveys. In the measurement, antennas are scanned vertically, yielding data with high resolution in the vertical direction but relatively poor resolution in the horizontal, which makes it difficult to determine the horizontal location of objects with high accuracy. One can achieve higher resolution in the horizontal direction by using higher frequencies or shorter pulsewidths at the expense of the detectable range.

Numerous imaging, tomography, and inversion techniques have been studied for borehole measurements using two or more wells, i.e., cross-hole measurements. For instance, the

technique proposed in [1] uses a forward–backward time-stepping (FBTS) method and can successfully reconstruct property distributions of a medium from synthetic noise-free and noisy data. This method, however, requires a large number of iterations to solve the inverse problem in time domain. Jia *et al.* [2] proposed a hybrid algorithm that combines generic and Levenburg–Marquardt algorithms in order to reduce the search region and to optimize the physical parameters. In contrast, the method described in [3] solves inverse problems in the frequency domain to obtain many physical parameters. These techniques iteratively modify the model and compare modeled data to measured data. Since most conventional inversion techniques deal with the overall wavefields, they are still computationally expensive and are not suitable for on-site data processing. As another approach, a reverse-time migration technique has been proposed, and it could successfully image a subsurface cavity [4]. However, it may not generally work well unless the measurements are under optimum conditions, e.g., low amounts of noise and relatively dense sampled traces.

Similar inversion techniques have been developed in other research fields such as medical engineering, where the technique of dipole tracing (DT) has been used to find electrical dipoles in the human brain and heart tissue for biological activity measurements [5], [6]. In this technique, the ideal potential distribution with assumed electric dipoles is calculated by the boundary element method, and it is compared with the data measured by many electrodes on the scalp or chest. The minimized squared difference between the measured and calculated data indicates true electric dipole locations. In this technique, since the object to be located is known, and almost the same model structure of the organs can always be used, solving the inverse problem is not difficult. While a target is known in most cases for geological surveys, we cannot however know how much inhomogeneity the subsurface medium has. Therefore, the robustness of the technique and the initial guess are rather important, and a large number of iterations is required. Moreover, they require very dense data to achieve an accurate result. It is difficult to carry out measurements to acquire appropriate data due to the spatial and temporal limitations of the surveys, especially by borehole radar in urban areas.

Buried pipes often present obstacles to subsurface constructions such as subways and tunnels. It is often difficult to determine the location from the documents drawn at the time of the original installation, making the design prior to new construction rather difficult. In this paper, a new inversion technique is proposed for a cylindrical structure, and it uses known parameters on the target explicitly. The proposed algorithm is demonstrated for a metallic pipe with synthetic data generated by the finite-difference time-domain (FDTD) method with a homogeneous and an inhomogeneous media

to show effectiveness and robustness. Then, it is applied to a field measurement data set. In addition, the inversion is applied to an air-filled cavity. Locating a cavity by borehole radar is still a challenging problem, and there are many studies using inversion [2], [3], imaging [4], and tomographic techniques [7], [8]. Finally, we interpret the results and discuss the potential and the further applications of our technique.

II. ALGORITHM OF THE INVERSION

A. Strategy of the Inversion

The technique tries to estimate the location of a buried metallic pipe and an air-filled cavity by the following procedure, using cross-hole fan measurement data (i.e., a transmitter is fixed at particular depths, and a receiver is scanned along the borehole axis). The object location is assumed, the first-arrival times are calculated for various transmitter and receiver positions, and the curve of the calculated first-arrival times is compared to that of the measured data. The calculation and comparison are repeatedly done while changing the assumed location. The assumed location that yields a curve shape most similar to that of the measured curve is determined to be the location of the object.

The inversion method is essentially the same as other inversion techniques with respect to the comparison of calculated and measured signals. One difference is that this technique deals only with first-arrival times. To perform the comparison, times representing the first arrivals need to be selected. It is the most important feature in the algorithm in that the selected first-arrival times do not have to be true because the comparison focuses on the shape of their curves. Hence, the inversion is almost independent of the method of first-arrival picking. Another difference is that this technique just estimates a location, and it does not image anything. Therefore, this technique requires less computing resources and fewer data sets. Moreover, it can use known information efficiently and explicitly, which is the reason it can work well even if it uses rather simple calculations. Conversely, conventional inversion techniques must consider complex scatterings to obtain an accurate image. Modeling with less realistic scattering mechanisms leads to errors and loss of accuracy, meaning that the conventional inversion techniques are much more sensitive to error by model inaccuracies than this technique.

B. Calculation of Approximated First-Arrival Times

1) Metallic Pipe: In general, there is information available prior to the measurements. Such *a priori* information is very important and helpful for the measurements and interpretations, and it should be utilized as much as possible. In this technique, we suppose that the following information is known:

1) material of the object;
2) dimension of the object.

Moreover, the following must be known when boreholes are drilled:

1) approximate location of the object;
2) direction of the object;
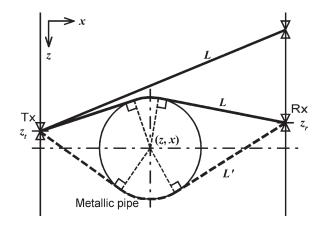3) separation between two boreholes.

Fig. 1. Two-dimensional geometry of a cross-hole measurement for a buried metallic pipe.

Such information simplifies the inversion problem. With the information, an approximated first-arrival time can easily be calculated with an assumption that the surrounding medium is homogeneous and the cylindrical object is perpendicular to the interborehole plane.

In the case of a metallic pipe as two-dimensionally (2-D) illustrated in Fig. 1, the shortest propagation path gives a first arrival. The shapes of the first-arrival curves resulting from those paths are different for various locations of the pipe, transmitter, and receiver. If the pipe is located between the antennas, a signal cannot pass through the metallic pipe and propagates along the curved surface of the pipe. As shown in Fig. 1, there are two possible propagation paths of such creeping waves: L and L'. Since the inversion uses only the first-arrival time, the shorter one, which is L in this case, is selected. The length of path L with the buried pipe at a particular location (z, x) can be represented as a function of object location (z, x) and transmitter and receiver depths z_t and z_r. The approximated first-arrival time with a particular configuration can be given by

$$t_{\text{cal}}(z, x, z_t, z_r) = L(z, x, z_t, z_r)/v \tag{1}$$

where v is the velocity of the electromagnetic wave in the subsurface medium, and it is assumed that the creeping wave propagates with velocity v.

2) Cavity: Here, a model is considered to keep the calculations simple for an air-filled cavity with an assumption that the shape of the cavity in the considering plane is a circle. Only Snell's law is taken into account in deciding the propagation paths, as shown in Fig. 2. When a propagation path passes through the cavity, the approximated first-arrival time can be expressed as

$$t_{\text{cal}}(z, x, z_t, z_r) = (L_1 + L_2)/v + L_3/c \tag{2}$$

where L_1 and L_2 are the propagation lengths in the surrounding medium, L_3 is inside the cavity, and c is the velocity in the air. Since the velocity in the cavity is higher than that in the subsurface medium, it is possible that a first arrival given by a path L_1, L_2, and L_3 passing through the cavity is faster than that given by a straight path L' even though the straight path is shorter. Thus, the first-arrival times given by all the possible paths must be calculated, and the fast one must be selected.
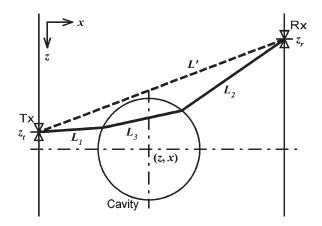
Fig. 2.   Two-dimensional geometry of a cross-hole measurement for an air-filled cavity.

C. Evaluation of Calculated First-Arrival Time Curve Shapes

The calculated first-arrival curves are compared with first-arrival curves from the measured data. The similarities of the curves can be calculated for various pipe locations, and the highest similarity indicates the true location. Picking an accurate first-arrival time from a measured trace is difficult because of the noise, limited frequency bandwidth, and zero-time offset in a time-domain system. In general, the results of techniques using selected first-arrival times strongly depend on the quality of the picks. Here, two schemes for evaluating the similarity of two curves, focusing on their shapes, are proposed, and they ideally do not depend on the manual picks. The first scheme works by taking the error of the curve gradients, whereas the second uses one-dimensional correlation. Hereafter, they are termed as the gradient error scheme and the correlation scheme, respectively.

1) Gradient Error Scheme: It is easy to select the time $t_{\mathrm{meas}}(z_t, z_r)$ at the maximum amplitude in a measured trace, where z_t and z_r denote the depths of a transmitter and a receiver, respectively. The times $t_{\mathrm{meas}}(z_t, z_r)$ obtained by this manner are no longer true first-arrival times, whereas it is assumed that the curves connecting the selected times are parallel to the true first-arrival curves. Then, the similarity between the measured curves $t_{\mathrm{meas}}(z_t, z_r)$ and the calculated curves $t_{\mathrm{cal}}(z, x, z_t, z_r)$ can be evaluated by taking the error $e(z, x, z_t)$ between the gradients of $t_{\mathrm{meas}}(z_t, z_r)$ and $t_{\mathrm{cal}}(z, x, z_t, z_r)$, which is given by the integration along the receiver depth z_r and expressed as

$$e(z, x, z_t) = \frac{1}{N_r} \int dz_r \left| \partial_{z_r} t_{\mathrm{meas}}(z_t, z_r) - \partial_{z_r} t_{\mathrm{cal}}(z, x, z_t, z_r) \right| \tag{3}$$

where N_r is the number of receivers for a transmitter. This error can be calculated for each transmitter depth. The low value indicates the high similarity of the curves, indicating the high probability of the object location. A total error for a series of transmitter depths $e_{\mathrm{total}}(z, x)$ is given by physical conjunction of the errors $e(z, x, z_t)$ and can be calculated by integration along the transmitter depth z_t and expressed as

$$e_{\mathrm{total}}(z, x) = \frac{1}{N_t} \int dz_t e(z, x, z_t) \tag{4}$$

where N_t is the number of transmitters used in this calculation. A lower error region in the distribution of the total error $e_{\mathrm{total}}(z, x)$ indicates a higher probability of the location of the object.

2) Correlation Scheme: To take a cross correlation, a reference must be constructed from the calculated first arrival $t_{\mathrm{cal}}(z, x, z_t, z_r)$; here, we construct a binary reference

$$H(z, x, z_t, z_r, t) = \delta\left(t - t_{\mathrm{cal}}(z, x, z_t, z_r)\right). \tag{5}$$

The one-dimensional (1-D) cross correlation between the reference $H(z, x, z_t, z_r, t)$ and the measured data $S(z_t, z_r, t)$ is calculated to time t, and the similarity $R(z, x, z_t)$ of the first-arrival curves at a transmitter depth z_t is defined as the maximum absolute value of the integration along the receiver depth of the correlation values and is given by

$$
\begin{aligned}
&R(z, x, z_t)\\
&= \frac{1}{N_r} \max_t \left| \int \int d\tau \, dz_r S(z_t, z_r, \tau) H(z, x, z_t, z_r, t - \tau) \right|. \tag{6}
\end{aligned}
$$

To obtain the total correlation $R_{\mathrm{total}}(z, x)$, those similarity values are integrated along the transmitter depth z_t as

$$R_{\mathrm{total}}(z, x) = \frac{1}{N_t} \int dz_t R(z, x, z_t). \tag{7}$$

In the distribution of the total correlation $R_{\mathrm{total}}(z, x)$, a higher correlation region indicates a higher probability of the object location. The amplitude of a measured signal directly relates to the correlation value, and each signal has different amplitudes due to the different lengths of propagation paths and the radiation patterns of the antennas. Therefore, each signal $S(z_t, z_r, t)$ has to be normalized because the weights of the correlation values have to be the same in order to integrate (6) and (7). In this scheme, the similarities can be evaluated without picking operations.

By the schemes, we can avoid the error of selecting the true first-arrival times from the measured data, and we do not need to consider how to define them. This makes the inversion technique simple, robust, and easy to operate. Both schemes have advantages and disadvantages. The gradient error scheme requires picks of times representing first arrivals, and sometimes it has less objectivity. However, if the curves can be determined successfully, this technique works well and is robust and stable. In the correlation scheme, one does not need to determine the curves, whereas the result strongly depends on a reference signal. If the reference signal is constructed unsuccessfully, this technique is very sensitive to noise in the measured signals. Of course, a measured or a synthetic wavelet such as a Gaussian pulse and a sync function can be employed as a reference signal. Nevertheless, the technique must have more parameters to be specified, making it less objective and usable. Thus, binary reference signals consisting of only 0 and 1 are used in the formation and in the succeeding discussions.

III. EXAMPLES WITH SYNTHETIC DATA

The inversion scheme is applied to synthetic data generated by a three-dimensional (3-D) FDTD simulation with the configuration shown in Fig. 3. The parameters used in the
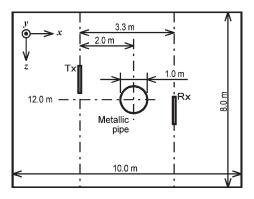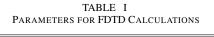
Fig. 3. Model for the FDTD calculation at $y = 5.0$ m. The transmitter is set at depths of 11.0, 11.5, 12.0, 12.5, and 13.0 m, and the receiver is set at depths in the range of 10.0–14.0 m with 0.1-m steps.

TABLE I
PARAMETERS FOR FDTD CALCULATIONS

Cell size	$0.1 \times 0.1 \times 0.1$ m
Number of cells	$100 \times 100 \times 80$
Time step	0.19258078 ns
Number of time steps	1500
Boundary condition	10 layers PML
Excitation pulse	2nd derivative Gaussian pulse
Transmitter depth	11.0-13.0 m, 0.5 m step
Receiver depth	10.0-14.0 m, 0.1 m step

Fig. 4. Radar profiles obtained by FDTD calculations with a homogeneous medium model. The transmitter is set at depths of (a) 11.0, (b) 11.5, (c) 12.0, (d) 12.5, and (e) 13.0 m. The target is a metallic pipe having a diameter of 1.0 m, and it is located at a depth of 12.0 and 2.0 m from the transmitter borehole.

simulation are shown in Table I. A second-derivative Gaussian pulse is used as the source excitation, and the frequency range is 10–200 MHz, which gives a wavelength of 1–2 m in a medium with a permittivity of $20 \, \varepsilon_0$. A 1.0-m-diameter metallic pipe is modeled at a depth of 12.0 and 2.0 m apart from the transmitting borehole.

A. Homogeneous Medium Model

We set a constant permittivity and conductivity of $20 \, \varepsilon_0$ and 0.01 S/m, respectively, for a homogeneous medium model. The modeled radar profiles are shown in Fig. 4. The parameters used in the inversion calculations are summarized in Table II. In the gradient error scheme, the times at positive maximum ampli-

TABLE II
INVERSION PARAMETERS FOR THE SYNTHETIC DATA WITH
THE HOMOGENEOUS MEDIUM MODEL

	Gradient error scheme	Correlation scheme
Used Tx depth	All depths	All depths
Used Rx depth	All depths	All depths
Calculation step	0.1 m in distance, 0.1 m in depth	0.1 m in distance, 0.1 m in depth
Assumed permittivity	20	20
Arrival time picking	Times at maximum positive amplitude	-
Reference signal	-	1 pixel rectangular pulse

Fig. 5. Error distributions calculated from synthetic data with the homogeneous medium model for the transmitter at depths of (a) 11.0, (b) 11.5, (c) 12.0, (d) 12.5, and (e) 13.0 m.
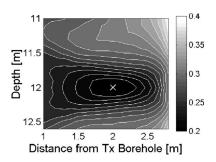

Fig. 6. Total error distribution obtained by the summation of all the errors shown in Fig. 5. The white cross indicates the minimum error, and it is at a depth of 12.0 and 2.0 m from the transmitting borehole.

tudes are selected from the data. Fig. 5 shows the errors for each transmitter depth. In those figures, the low-error regions are not localized and spreading along the lines connecting the transmitter positions and the center of the pipe, and the location cannot be clearly estimated. Fig. 6 shows the distribution of the total error obtained by summation of all the errors. The distribution has a localized low-error region. The minimum error indicates a depth of 12.0 m and a horizontal distance of 2.0 m apart from the transmitter borehole. It is exactly the same as the location of the modeled pipe. In the correlation scheme, the reference signals are constructed as one-pixel rectangular pulses, i.e., one pixel is set to 1 or, otherwise, 0 in a trace. The correlation distributions for five transmitter depths are shown in Fig. 7. Similar to the gradient error scheme, the high-correlation regions are spreading. Fig. 8 shows the summed correlation distribution. The high-correlation region is localized in this figure, and the maximum value is at a depth of 12.0 and 2.0 m from the transmitting borehole. It is also exactly the same as the pipe location. In the inversion operations, the
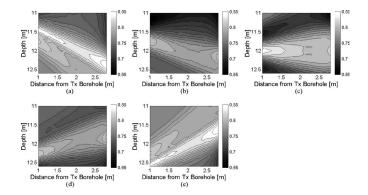
Fig. 7. Correlation distributions from the synthetic data with the homogeneous medium for the transmitter at depths of (a) 11.0, (b) 11.5, (c) 12.0, (d) 12.5, and (e) 13.0 m.
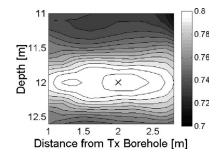

Fig. 8. Total correlation distribution obtained by the summation of all the distributions shown in Fig. 7. The black cross indicates the maximum correlation, and it is at depths of 12.0 and 2.0 m from the transmitting borehole.
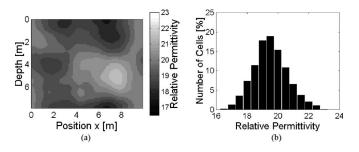

Fig. 9. Relative permittivity distribution of the simulated heterogeneous medium. (a) Vertical slice at $y = 5.0$ m and (b) histogram of the permittivities.

pipe location is assumed every 0.1 m in both the vertical and horizontal directions.

B. Heterogeneous Medium Model

For demonstrating a more realistic situation, a heterogeneous medium is simulated in a 3-D space employing a stochastic fractal model [9]. The vertical slice of the simulated heterogeneous model and its histogram are shown in Fig. 9. The model consists of 14 permittivities, ranging from 16.5–23.0 ε_0, and a constant conductivity of 0.01 S/m. The distribution of permittivities has a mean of 19.5 ε_0, a standard deviation of 1.1 ε_0, and a correlation length of 5 m. For the inversion, we assume a homogeneous medium of 20.0 ε_0. Fig. 10 shows the total error and correlation distributions. Although the localized regions are deformed compared to the homogeneous medium case shown in Figs. 6 and 8, they possess the minimum error and the maximum correlation values at the exact modeled location.
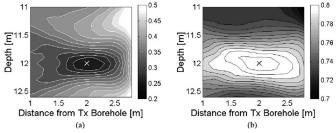

Fig. 10. Results of the inversion technique from synthetic data with the heterogeneous model using (a) the gradient error scheme and (b) the correlation scheme. The minimum error marked by a white cross in (a) indicates a depth of 12.0 and 2.0 m from BH1. The maximum correlation value marked by a black cross in (b) indicates a depth of 12.0 and 2.0 m from BH1.
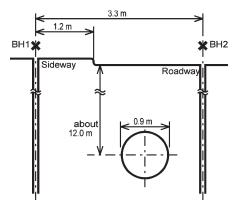

Fig. 11. Geometrical sketch of the site for the field measurements in Sendai, Japan, in 2004.

IV. APPLICATION TO MEASURED DATA

A. Metallic Pipe

Field measurements were carried out in an urban area in the city of Sendai, Japan, in September 2004. The target is a metallic pipe for water supply having a diameter of 0.9 m and is buried at a depth of about 12.0 m. There were two boreholes with a separation of 3.3 m on both sides of the pipe, as shown in Fig. 11. We carried out various borehole radar measurements such as single-hole, cross-hole parallel, and cross-hole fan measurements using a radar system developed by Tohoku University, which is a vector-network-analyzer-based stepped-frequency continuous-wave (SFCW) radar system [10]. A frequency range of 2–402 MHz was used in the measurements, and dipole antennas having a length of 900 mm were used as a transmitter and a receiver. The dominant frequency of the measured data is about 80 MHz. Fig. 12 shows the radar profiles obtained by the cross-hole fan measurements, in which the transmitter was set in borehole BH1 at depths of 11.0, 11.5, 12.0, 12.5, and 13.0 m and the receiver was scanned at depths in the range of 10.0–14.0 m with a 0.1-m step in BH2.

Since discontinuities can be found in the radar profiles, the subsurface may be layered with two kinds of media. Thus, a two-layer model is constructed for a 2-D transverse electric (TE) FDTD method in order to obtain the approximated arrival times. The layer interface is set at a depth of 12.5 m, and the relative permittivities are assumed to be 25 ε_0 and 20 ε_0 for the upper and lower media, respectively, as shown in Fig. 13.
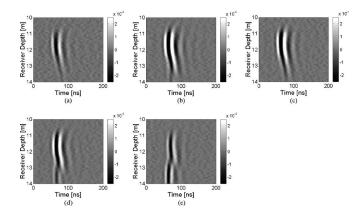
Fig. 12. Radar profiles obtained by cross-hole fan measurements for a buried metallic pipe in Sendai, Japan, in 2004. The transmitter was set in BH1 at depths of (a) 11.0, (b) 11.5, (c) 12.0, (d) 12.5, and (e) 13.0 m.
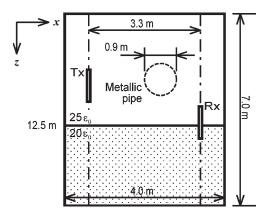

Fig. 13. Model for the 2-D TE FDTD calculation in order to obtain the approximated arrival time. The cell size is 0.1 m × 0.1 m. The permittivity of the upper and lower layers is set to 25 ε_0 and 20 ε_0, respectively.

TABLE III
INVERSION PARAMETERS FOR THE MEASURED
DATA WITH THE METALLIC PIPE

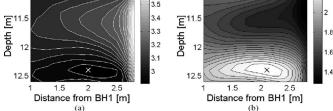|	Gradient error scheme	Correlation scheme
Used Tx depth	11.0, 11.5, 12.0, 12.5, 13.0 m	11.0, 11.5, 12.0, 12.5, 13.0 m
Used Rx depth	11.0–13.0 m	11.0–13.0 m
Calculation step	0.1 m in distance, 0.1 m in depth	0.1 m in distance, 0.1 m in depth
Arrival time picking	Threshold at 40 % of maximum amplitude	-
Reference signal	-	3 pixel rectangular pulse

Fig. 14. Results of the inversion for the pipe using (a) the gradient error scheme and (b) the correlation scheme with field measurement data. The minimum error in (a) indicates a depth of 12.4 and 2.0 m from BH1. The maximum correlation value in (b) indicates a depth of 12.4 and 2.1 m from BH1.

In the FDTD calculations, the cell size is 0.1 m × 0.1 m, and the time step is 0.1 ns. An absorbing boundary condition (ABC) is not implemented in the FDTD model, and the calculation is
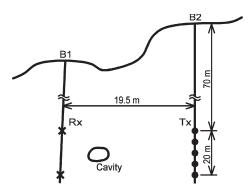

Fig. 15. Geometrical sketch of the site for the field measurements in Korea in 2000.
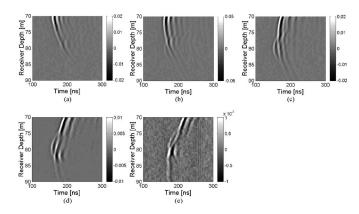

Fig. 16. Radar profiles obtained by the cross-hole fan measurements for an air-filled cavity in Korea in 2000. The transmitter is set at depths of (a) 70, (b) 75, (c) 80, (d) 85, and (e) 90 m.
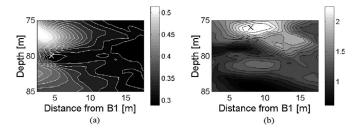

Fig. 17. Results of the inversion for the air-filled cavity using (a) the gradient error scheme and (b) the correlation scheme. The minimum error in (a) indicates a depth of 80 and 4.5 m from B1.

terminated when a first arrival is observed. An approximated arrival time is selected from the measured data by a threshold at 40% of the maximum amplitude in each trace for the gradient error scheme. The threshold is determined as it gives smooth curves. Three-pixel rectangular pulses are used as the reference for the correlation scheme, as summarized in Table III. The pipe locations are assumed with 0.1-m steps in both schemes. Both results shown in Fig. 14 indicate similar locations, a depth of 12.4 and 2.0 m from BH1 by the gradient error scheme, and a depth of 12.4 and 2.1 m from BH1 by the correlation scheme. Those locations agree well with the known information that the pipe is close to borehole BH2 rather than BH1.

B. Cavity

Data for locating an air-filled cavity were acquired in Korea, in 2000 [4]. The vertical profile of the site is illustrated in

TABLE IV
INVERSION PARAMETERS FOR THE MEASURED DATA WITH THE CAVITY

	Gradient error scheme	Correlation scheme
Used Tx depth	75, 80, 85 m	75, 80, 85 m
Used Rx depth	73-83 m (for Tx at 75 m)	75-85 m
	73-85 m (for Tx at 80 m)	
	73-84 m (for Tx at 85 m)	
Calculation step	0.5 m in distance, 0.5 m in depth	0.5 m in distance, 0.5 m in depth
Assumed permittivity	5.0	5.0
	Threshold:	
Arrival time picking	30 % (for Tx at 75, 80 m)	-
	40 % (for Tx at 85 m)	
Reference signal	-	3 pixel rectangular pulse

Fig. 15. The radar system used in the measurements is also our radar system [11], and dipole antennas were used as a transmitter and a receiver. The dominant frequency of the data is about 65 MHz. The site consists of a cavity between two boreholes separated by 19.5 m, and the cavity has a diameter of about 3.0 m. For the cross-hole fan measurements, the transmitter was placed in borehole B2 in a range of 70–90 m for every 5m, and the receiver scans in borehole B1 between 70–90 m for every 0.125 m. The profiles are shown in Fig. 16, and we can easily find anomalies due to a cavity around a depth of 80 m.

Fig. 17 shows the results of the inversion. As summarized in Table IV, the data acquired by the transmitter at depths of 75, 80, and 85 m are used. In Fig. 17(a), we can see a well-localized region and the minimum error at a depth of 80 and 4.5 m from B1. It is in good agreement with the imaging result of [4]. However, in Fig. 17(b), the maximum correlation is at a depth of 75.5 and 8 m from B1. The reason for the inaccurate result is that the correlation has a high response not only at first arrivals but also at other scattered waves in the measured data because it takes the cross correlation between the binary reference and raw measured data for a cavity, which possesses relatively high-energy scattered wave compared to the metallic pipe case. Thus, the gradient error scheme is suitable for a cavity.

V. DISCUSSION

A result of a borehole radar tomography calculated from the same data, considering straight ray paths, is shown in Fig. 18. It is very noisy and almost impossible to discern anything from the image. This unsuccessful result is due to the sparse sampling and small measurement region. In addition, tomography can generally work well for an object whose properties are gradually changed, but it cannot clearly image an object that possesses high contrast of properties to the surrounding medium such as an artificial object like a metallic pipe. However, the inversion can work well for such objects rather than low-contrast objects because the deformation of the arrival time curve is greater with a high-contrast object. Therefore, the inversion technique is more suitable in determining a buried pipe location than the tomographic technique in this situation.

Since the changes of arrival time curves by an air-filled cavity is larger than that by the metallic pipe, the localization in the error distribution is better. Thus, the technique is more suitable for a cavity than a metallic pipe. The result by the
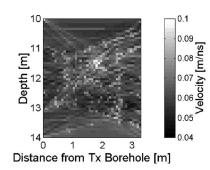

Fig. 18. Distribution of the propagation velocity obtained by travel time tomography, considering straight ray paths with the measured data for the metallic pipe. There is no clear contrast in this image, and it is almost impossible to get any valid information from this result.

correlation scheme is inaccurate, and it seems that the scheme is not suitable for a cavity. It would work accurately if the reference includes not only first arrivals but also scattered wavefields, e.g., by means of FDTD for a forward modeling. Another possible solution is that the cross correlation is taken between the binary reference and the binary data, which is constructed by selecting first-arrival times from the measured data. By this manner, the scattered wavefields in the measured data are eliminated, and the cross correlation can be taken only for first arrivals.

The inversion of the synthetic data for a metallic pipe needs only 15% of the computation time of an algebraic reconstruction technique (ART)-based straight ray tomography whose terminate condition is within 0.001 ns of the maximum update. In this case, the forward model is obtained by simple geometric calculations; thus, the computation is much faster than that of the tomographic technique. In fact, the forward model calculation by FDTD in the case of the measured data takes more time to compute. However, we can prepare the models prior to measurements if a piece of information is available beforehand, and the on-site computation (i.e., evaluations of curve shapes) can be done very quickly.

VI. CONCLUSION

An estimation technique of the buried location for a cylindrical structure with a parametric approach is discussed, and it is applied to the synthetic and measured data. For the synthetic data with both homogeneous and heterogeneous media, the technique can retrieve the exact location of a pipe. It indicates

that the technique is rather robust against the heterogeneity. Moreover, it can estimate the pipe and cavity location for measured data in agreement with known information, in cases where travel time tomography cannot image due to sparse sampling and a small measurement region. This shows that our technique is more suitable for the estimation of an object location with sparse data when certain information on the object is known. Further, it only requires rather simple calculations that can be done quickly. The result shows an obvious solution unlike other imaging techniques, which generally need interpretations of the resulting image. Therefore, the method is robust, simple, stable, and easy to operate. It can easily be applied on-site, and it is an enormous advantage for the practical use for underground surveying.

The technique, which delays or quickens first arrivals with small modifications of the forward model, can be applied to other bistatic radar transmission measurements such as vertical radar profiling (VRP) measurements and to other objects. For two or more objects, a more complex forward model has to be considered. In those complicated cases, FDTD can be used for the forward modeling as we used in the case of the metallic pipe. For FDTD, two dimensions may be enough; it does not need an ABC and extra calculation space, and it can be terminated when the first arrival is observed. It still has less computing costs. Therefore, it possesses high potential for use in various applications.

ACKNOWLEDGMENT

REFERENCES

[1] T. Takenaka, H. Zhou, and T. Tanaka, "Inverse scattering for a three-dimensional object in the time domain," *J. Opt. Soc. Amer. A, Opt. Image Sci.*, vol. 20, no. 10, pp. 1867–1874, Oct. 2003.

[2] H. Jia, T. Takenaka, and T. Tanaka, "Time-domain inverse scattering method for cross-borehole radar imaging," *IEEE Trans. Geosci. Remote Sens.*, vol. 40, no. 7, pp. 1640–1647, Jul. 2002.

[3] H. K. Choi and J. W. Ra, "Detection and identification of a tunnel by iterative inversion from cross-borehole CW measurements," *Microw. Opt. Technol. Lett.*, vol. 21, no. 6, pp. 458–465, Jun. 1999.

[4] H. Zhou and M. Sato, "Subsurface cavity imaging by crosshole borehole radar measurements," *IEEE Trans. Geosci. Remote Sens.*, vol. 42, no. 2, pp. 335–341, Feb. 2004.

[5] B. He, T. Musha, Y. Okamoto, S. Homma, Y. Nakajima, and T. Sato, "Electric dipole tracing in the brain by means of the boundary element method and its accuracy," *IEEE Trans. Biomed. Eng.*, vol. BME-34, no. 6, pp. 406–414, Jun. 1987.

[6] Y. Okamoto, Y. Teramachi, T. Musha, H. Tsunakawa, and K. Harumi, "Moving multiple dipole model for cardiac activity," *Jpn. Heart J.*, vol. 3, no. 3, pp. 293–304, May 1982.

[7] S. K. Park, H. K. Choi, and J. W. Ra, "Underground tomogram from cross-borehole measurements," *Microw. Opt. Technol. Lett.*, vol. 18, no. 6, pp. 402–406, Aug. 1998.

[8] A. Becht, J. Tronicke, E. Appel, and P. Dietrich, "Inversion strategy in crosshole radar tomography using information of data subsets," *Geophysics*, vol. 69, no. 1, pp. 222–230, Jan./Feb. 2004.

[9] B. Lampe and K. Holliger, "Effects of fractal fluctuations in topographic relief, permittivity and conductivity on ground-penetrating radar antenna radiation," *Geophysics*, vol. 68, no. 6, pp. 1934–1944, Nov./Dec. 2003.

[10] K. Takahashi, S. Liu, and M. Sato, "Interferometric borehole radar system," in *Proc. 9th Int. Conf. GPR*, Santa Barbara, CA, Apr. 2002, vol. 4758, pp. 19–24.

[11] T. Miwa, M. Sato, and H. Niitsuma, "Subsurface fracture measurement with polarimetric borehole radar," *IEEE. Trans. Geosci. Remote Sens.*, vol. 37, no. 2, pp. 828–837, Mar. 1999.

Kazunori Takahashi (S'05) received the B.E. degree in mechanical engineering from Yamagata University, Yamagata, Japan, in 2001, and the M.E. and Ph.D. degrees in geoscience engineering from Tohoku University, Sendai, Japan, in 2003 and 2006, respectively.

He is currently a Research Associate with the Center for Northeast Asian Studies, Tohoku University. His current research interests include the development of ground-penetrating radar and borehole radar systems, and their application and analysis using radar polarimetry and interferometry, inverse problem, and landmine detection by ground-penetrating radar for humanitarian demining.

Motoyuki Sato (S'79–M'80–SM'02) received the B.E., M.E., and Dr.Eng. degrees in electrocommunication and information engineering from Tohoku University, Sendai, Japan, in 1980, 1982, and 1985, respectively.

He joined the Faculty of Engineering, Tohoku University, in 1985. From 1988 to 1989, he was a Visiting Researcher with the Federal Institute for Geoscience and Natural Resources (BGR), Hannover, Germany. He is currently a Professor with the Center for Northeast Asian Studies, Tohoku University. He is also an Honorary Professor of the Mongolian University of Science and Technology, Ulanbator, Mongolia, China; a Member of the World Academy of Chingges Khaan, Mongolia; a Guest Professor of Jilin University, Changchun, China; and a Principal Investigator of the Advanced Land Observation Satellite calibration/validation and polarimetric airborne SAR. His current research interests include transient electromagnetics and antennas, radar polarimetry, ground-penetrating radar and its applications to environment studies and humanitarian demining, borehole radar, electromagnetic logging, and interferometric and polarimetric SAR.

Dr. Sato was a recipient of the Best Poster Award of the SPWLA in 1994 and the Society of Exploration Geophysicists of Japan (SEGJ) award in 1999. He served as a Technical Chairman of the 6th International Conference on Ground Penetrating Radar (GPR'96), Sendai, Japan, and a Chairperson of the SEGJ International Symposium in 2006. He is an AdCom Member of the IEEE GRSS and a Chairperson of the Japan Chapter of the IEEE GRSS, both during 2006–2007.